Nuclear Engineering and Design 262 (2013) 189–200

Contents lists available at SciVerse ScienceDirect

Nuclear Engineering and Design

journal homepage: www.elsevier.com/locate/nucengdes

The numerical computation of seismic fragility of base-isolated Nuclear Power Plants buildings

Federico Perotti [a], Marco Domaneschi [a,*], Silvia De Grandis [b]

[a] Department of Civil and Environmental Engineering, Politecnico di Milano, Milan, Italy
[b] SINTEC srl, Bologna, Italy

highlights

- Seismic fragility of structural components in base isolated NPP is computed.
- Dynamic integration, Response Surface, FORM and Monte Carlo Simulation are adopted.
- Refined approach for modeling the non-linearities behavior of isolators is proposed.
- Beyond-design conditions are addressed.
- The preliminary design of the isolated IRIS is the application of the procedure.

article info

Article history:
Received 19 October 2012
Received in revised form 10 April 2013
Accepted 19 April 2013

abstract

The research work here described is devoted to the development of a numerical procedure for the computation of seismic fragilities for equipment and structural components in Nuclear Power Plants; in particular, reference is made, in the present paper, to the case of isolated buildings. The proposed procedure for fragility computation makes use of the Response Surface Methodology to model the influence of the random variables on the dynamic response. To account for stochastic loading, the latter is computed by means of a simulation procedure. Given the Response Surface, the Monte Carlo method is used to compute the failure probability. The procedure is here applied to the preliminary design of the Nuclear Power Plant reactor building within the International Reactor Innovative and Secure international project; the building is equipped with a base isolation system based on the introduction of High Damping Rubber Bearing elements showing a markedly non linear mechanical behavior. The fragility analysis is performed assuming that the isolation devices become the critical elements in terms of seismic risk and that, once base-isolation is introduced, the dynamic behavior of the building can be captured by low-dimensional numerical models.

1. Introduction

The introduction of isolation systems in the design of strategic buildings is likely to become, in the next future, a widespread seismic protection measure. In fact, the anticipated better performance, when compared to the one of traditional buildings, in terms of acceleration response to design seismic actions, makes isolation techniques a very attractive choice for buildings whose functionality after the event is of utmost importance.

Two American Society of Civil Engineers standards (ASCE, 2000, 2005) report on the analysis and design of Nuclear Power Plants (NPP). The former in particular includes rudimentary provisions for the analysis and design of seismic isolation systems. In its revised version under development, it will comprise new prescriptions on the mathematical models for the non linear behavior of the isolation system and the nuclear buildings, which will satisfy the risk-informed goals of ASCE/SEI 43-05 (Huang et al., 2012). Furthermore, instructions and recommendations for qualifying control devices for Nuclear Power Plants application are also expected.

Such design prospect is the typical case of reactor buildings in future Nuclear Power Plants, where the adoption of isolation systems seems to be almost mandatory if the frequency of earthquake-induced accident scenarios must drop to values of the order of E-08/ry to make the seismic risk of the same order of magnitude if compared to risk related to internal events (Carelli et al., 2004). In this respect, isolation systems based on High Damping Rubber Bearings (HDRB) represent an attractive design solution, given their diffusion and proven reliability; in (Forni et al., 2010;

* Corresponding author at: Department of Civil and Environmental Engineering, Politecnico di Milano, Piazza Leonardo da Vinci 32, Milan, Italy. Tel.: +39 02 2399 4267; fax: +39 02 2399 4220.
E-mail address: marco.domaneschi@polimi.it (M. Domaneschi).

0029-5493/$ – see front matter © 2013 Elsevier B.V. All rights reserved.
http://dx.doi.org/10.1016/j.nucengdes.2013.04.029

Bianchi et al., 2011a,b) the application of this solution to the Nuclear Steam Supply System (NSSS) building designed within the International Reactor Innovative and Secure (IRIS) international project (Carelli et al., 2004) is described and some preliminary results are given. These results show how the isolation system is extremely effective in reducing the horizontal seismic acceleration transmitted to all structural and equipment components inside the building, this resulting in significant advantages for the design and standardization of the equipment. It must be observed, however, that in such conditions the isolation devices themselves are prone to become the critical components in terms of seismic fragility, since the response attenuation is obtained as the result of large relative displacements between the building and the foundation. Therefore, the need arises to assess the risk associated to the failure of the isolators, this being obviously related to "beyond design" loading conditions. In addition, the impact of the isolated superstructure on surrounding buildings or geotechnical structures is a critical aspect as well to be considered in the base isolated NPP configuration.

When the problem of risk evaluation is addressed, the fundamental role played by the hazard definition in the estimation of the seismic-induced CDF is immediately evident; both randomness and uncertainty, however, significantly affect also the evaluation of structural behavior under extreme loads and thus of seismic reliability. Though randomness cannot be avoided, since is inherent to most of the input data of the analysis, uncertainties, being related to the lack of complete and accurate knowledge about models and methods, must be reduced as much as possible by refining analysis procedures.

In light of the above considerations, the research activity described in the present paper is devoted to the probabilistic evaluation of the seismic performance of a NPP reactor building encompassing passive seismic isolation. An innovative procedure for fragility estimation (De Grandis et al., 2009) will be summarized in the next section focusing on the isolated case; in the following, the criteria adopted for a refined mechanical modeling of the nonlinear behavior of the isolators will be described. An example of application to a real life case will be finally shown.

2. The fragility analysis of NPP components

Starting from the 80s the seismic fragility of NPP components has been computed by means of the simplified but well consolidated procedure by Kennedy and co-workers (Kennedy et al., 1980; Kennedy and Ravindra, 1984), based on the structural performance at the SSE (Safe Shutdown Earthquake) and on the estimation of actual vulnerability by the introduction of a set of safety coefficients. Each coefficient accounts for both the randomness and/or uncertainty related to a particular aspect or parameter of the analysis and for its influence on the seismic performance; all coefficients are assumed to follow a lognormal distribution whose properties are defined by engineering judgment, experience and previous parametric studies.

Aim of the research here described is to develop a more sophisticated procedure, able to eliminate part of the uncertainties and thus of the conservatism which is inherent to the traditional methods, especially in the way the actual dynamic behavior of the building structure and the effect of random aspects/parameters are accounted for.

The proposed procedure (De Grandis et al., 2009) is based on classical methods of structural reliability analysis, as applied to systems with low-dimensionality, i.e. a limited number of random variables. In fact, as discussed in (De Grandis et al., 2009), the number of random aspects usually introduced in the fragility analysis of NPPs is of the order of 5–10 (ASCE, 2000 – Section A3.1, Table A1 "Parameters Considered in Fragility Analysis"). Even though each of these aspects (e.g. structural stiffness) should be described, in principle, by a large number of random variables (RVs), actually describing a stochastic field, we must consider that, if no local effect is of concern, the adoption, for each aspect, of a single RV representing a (spatial) average can be justified.

2.1. General formulation

Following the PEER (Pacific Earthquake Engineering Research) approach (Cornell and Krawinkler, 2000; Der Kiureghian, 2005), the annual failure rate for a mechanical component under seismic loading can be obtained from the integral:

$$P_f = \iint P\{DM > dm_f | EDP = edp\} p_{EDP} \times (edp|IM = im) p_{IM}(im) d(edp) d(im) \quad (1)$$

where DM is a Damage Measure, associated to the assumed limit state (dm_f denotes the damage level at failure), EDP is an Engineering Demand Parameter (support acceleration, relative displacement,...) expressing the level of the dynamic excitation imposed to the component due to the global seismic response of the structure (reactor building) and IM is an Intensity Measure (peak ground acceleration, spectral acceleration,...) characterizing the severity of the earthquake motion at the reactor site. As pointed out in (Der Kiureghian, 2005) all statistics in (1) must be intended in term of annual extreme values, so that the equation delivers a risk estimate in terms of annual probability of failure of the component.

In many practical cases the limit state can be directly defined in terms of the EDP value at failure edp_f, thus avoiding, or performing it at a different stage, the damage analysis step, i.e.:

$$P_f = \int P\{EDP > edp_f | IM = im\} p_{IM}(im) d(im) \quad (2)$$

where the integrand function can be written in terms of the following fragility function:

$$F(edp_f, im) = P\{EDP > edp_f | IM = im\} \quad (3)$$

When a traditional non-isolated building is considered a typical choice for edp within the above context is represented by the peak acceleration at the support point of critical equipment components; in this light, in (De Grandis et al., 2009) a numerical procedure for evaluating the seismic fragility was developed focusing on the cases in which linearity can be assumed for the building structural system. If a base-isolation system based on HDRB (High Damping Rubber Bearings) is introduced (see for example Forni et al., 2010) the acceleration values inside the building undergo a dramatic decrease. This is obtained at the price of significant relative displacements imposed to isolation devices, which are likely to become the "weakest link" in terms of seismic safety of the building; therefore the extreme value u of the relative displacement across the most strained isolator is a quite obvious first choice for the edp. The fragility function is thus expressed as:

$$F(edp_f, im) = P\{U > U_f | A_g = a_g\} = P_{exc}(U_f, a_g) \quad (4)$$

For a system under stochastic dynamic excitation, the associated limit state function can be expressed in the following "capacity minus demand" format:

$$g(\mathrm{X}, U, a_g) = C - D(\mathrm{X}, a_g) = U_f - U(\mathrm{X}, a_g) = 0 \quad (5)$$

In (5) U is the extreme value of relative displacement, i.e. a random variable whose distribution delivers, for fixed X, the result of the random vibration analysis, while U_f is the relative displacement leading to failure of the most strained isolator. Note that U_f can be defined either as a deterministic or a random parameter.

In (De Grandis et al., 2009) linearity of the building response was exploited, in the non-isolated case, for the probabilistic evaluation of the peak motion at the supports of an equipment component; differently, no linearization is herein exploited, since the behavior of HDRB is markedly non-linear, especially at the high level of deformations occurring in the beyond-design conditions which are typical of fragility analysis (Huang et al., 2012).

Once selected the probability distributions of X and U, the probability of exceeding the limit state (5), i.e. the integral

$$P_{exc}(U_f, a_g) = \int_{g<0} p_U(u, \mathrm{x})\, du\, d\mathrm{x} \tag{6}$$

could be computed, in principle, by direct application of the Monte Carlo Simulation (MCS) method; in fact the statistics of response $U(\mathrm{X})$ is algorithmically known, i.e. can be deterministically computed by structural dynamic analysis for every realization of the random variables X. It must be considered, however, that a huge computing time and cost would be required for running a non-linear dynamic analysis, as it is the case for isolated systems of the type here considered, for the number of evaluations which are necessary for MCS, especially for the estimation of small probabilities.

2.2. Limit-state approximation via Response Surface Methodology

For the above consideration, according to the well-established Response Surface Methodology (RS, Casciati and Faravelli, 1991; Faravelli, 1989; De Grandis et al., 2009), the "true" response function is replaced by a simple analytical representation. Here, assuming that the distribution of U can be described by its mean value μ_U and its standard deviation σ_U, the so called "Dual Response Surface" approach (Towashiraporn, 2004; Lin and Tu, 1995; De Grandis et al., 2009) has been adopted for modeling their dependency on X. Assuming that the same model can be used for the mean and the standard deviation the following response functions have been introduced:

$$\mu_U(\mathrm{X}) = \sum_{i=1}^{m} a_i z_i(\mathrm{X}) + \varepsilon_\mu; \qquad \sigma_U(\mathrm{X}) = \sum_{i=1}^{m} b_i z_i(\mathrm{X}) + \varepsilon_\sigma \tag{7}$$

where the a_i's and b_i's are coefficients to be estimated, the z_i's are usually polynomial functions and two "error" terms ε_μ and ε_σ are introduced as a zero mean random deviations (Pinto et al., 2004). The latter account for the variability of estimated quantities and for the lack of fit of the adopted model, i.e. for the inadequate analytical form of the RS's and for missing variables (i.e. not comprised in (7) though influencing the response). To compute the coefficients in (7) a number of experiments must be run according to the chosen experimental design; at each of them the random vibration problem can be addressed via either an analytical or a simulation approach. In a non-linear setting the second solution is the natural choice; consistently, a sample of ground motion realizations must be generated. If spectral parameters are comprised in X, the generation must be repeated at each experimental point. Given the realization of the excitation process, the extreme value of U is computed for each sample (e.g. via FE modeling and step-by-step analysis); the mean and standard deviation of U are then estimated. The procedure is repeated for all experimental points, leading to n observed values for the statistical parameters of $U(\mathrm{X})$.

We shall assume in the following that the experiments are performed in homogeneous conditions (i.e. differing for the x_i values only), that their results are independent and that the error terms are normal with constant variance; under these hypotheses an unbiased estimate of the coefficients a_i, b_i can be obtained by the Least Square (OLS) method, independently of the variance of the error terms ε_μ and ε_σ. An unbiased estimate of the latter can be subsequently obtained is defined via residual analysis. Once models (7) are established, MCS can be carried on. In the applications here shown a Central Composite Design has been adopted for defining the experimental points.

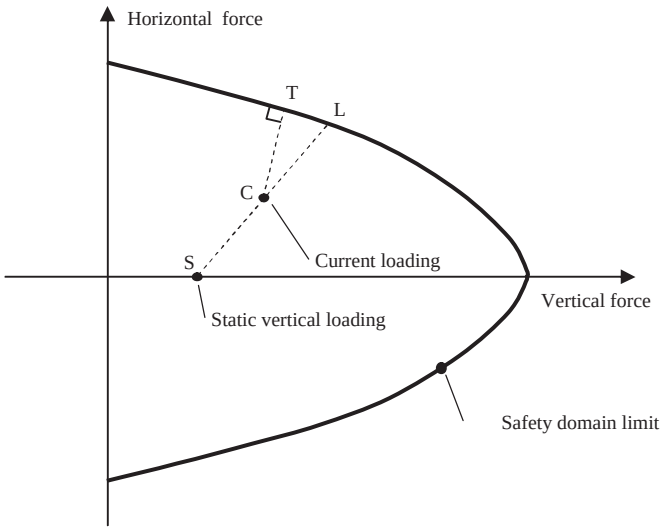

Fig. 1. Limit state function for the isolator.

Note that, differently from the linear case, analyzed in (De Grandis et al., 2009), the Response Surface evaluation must be repeated for every value of peak ground acceleration, this representing, potentially, a huge computational task. It can be considered, however, that in the isolated case the seismic behavior of the building can be captured, to the aim of evaluating the isolators' performance, by means of rather simple mechanical models; the latter, in fact, must be able to capture either rigid-body motions or a few global modes of the building above the isolators (Forni et al., 2010).

As a second option, under development in a parallel research, the "capacity minus demand" function (5) can be associated to a limit state function (Bianchi et al., 2011a,b) expressed in terms of horizontal and vertical loads acting on the most severely strained isolator; for typical HDRBs, made by alternate rubber and steel layers, the limit state considered is the "first damage" condition related to the attainment of an admissible peak tensile stress at the steel–rubber interface. In this light and with reference to Fig. 1, demand is here defined, at each instant, as the distance between the points describing the static vertical loading on the isolator (point S) and the current loading (point C), while capacity is computed as the total distance, measured along SC, between the static loading condition and the limit state surface (point L). Both are made non-dimensional with respect to the capacity so that the *edp* is represented by the ratio SC/SL, this being the inverse of the "instantaneous" safety factor, while the limit value edp_f takes a constant unit value. As an alternative, the actual distance CT can replace CL in the formulation of the safety factor.

The evaluation of the limit state domain, in terms of global vertical and horizontal forces, has been addressed in (Corradi et al., 2009; Bianchi et al., 2011c) as a consequence of delamination between steel and rubber layers of the device, by accounting a tension Mohr–Coulomb approach. Such failure mechanism occurs when high isolator shape factors (main horizontal dimensions over total rubber height) are recognized.

Note that considering first damage instead of actual failure in the formulation of the limit state surface appears to be consistent to the so-called ONSID (Onset of Significant Inelastic Damage) condition, often considered (ASCE, 2000, 2005; Huang et al., 2012) in nuclear design.

2.3. Refinement of the Response Surface approximation

Once a first evaluation of the Response Surfaces has been performed, an improved fitting can be pursued in the region of the failure domain where $p(\mathrm{x})$ is still relatively large, giving the largest contribution to the failure probability. An obvious choice, in this light, is to assume as design center the design or minimum norm point (Bucher and Burgund, 1990; Rajashekhar and Ellingwood, 1993); this is defined by transforming the RV's into the space of standard normal variables Y_i. Subsequently the limit-state function is expressed in the same space and its point which is closest to the origin is found; this can be also interpreted as the "most likely failure point". Obviously, the design point is not known when the analysis is started, so that an iterative refinement procedure is required in principle.

The above sketched procedure can be applied to the case at study for refining the Response Surfaces at each value of the seismic intensity (*PGA*) here considered. For developing a rational and cost-effective procedure, however, we can observe that the aim of the reliability evaluation is here the computation of the integral (2). Accordingly, and considering expression (4), we can write the annual probability of failure as:

$$P_f = \int F(edp_f, im)\, p_{IM}(im)\, d(im) = \int P_{exc}(U_f, a_g)\, p_{A_g}(a_g)\, d(a_g) \quad (8)$$

Once U_f is defined, either deterministically or as a random variable, a first evaluation of the P_{exc} function is available and a "prototype" site is chosen, the integrand function in (8) can be analyzed and the *PGA* range giving the maximum contribution to the total failure probability can be detected; from this very useful information can be inferred, not only for avoiding unnecessary RS refinements, but also for consistently calibrating mechanical and seismic excitation models.

Note that a similar reasoning was applied in (De Grandis et al., 2009), allowing, in a linear setting, for the definition and refinement of a single response function given in terms of response amplification. For a practical implementation, the FORM technique was adopted along with the Rosenblatt Transformation (Hoenbichler and Rackwitz, 1981); the same criterion can be here applied, by assuming a type I extreme-value distribution for the random variable U, accounting for the random character of the dynamic response.

3. Numerical modeling of isolation devices

As it is well known High Damping Rubber Bearings (HDRB) show a quite complex non-linear mechanical behavior, characterized by the *scragging* and *Mullins*' effects (stiffness and damping degradation) by the horizontal stiffness variation (due to temperature and axial load), by strain-rate dependence and aging.

Ozdemir and Wen models (Ozdemir, 1976; Wen, 1976) of smooth hysteresis are probably the most eclectic phenomenological model of isolation systems presented in the available literature. Thanks to their physical and mathematical consistency and the satisfactorily correspondence between the experimental and numerical results a number of developments have been established, from their original formulation, including new features and reproducing new technologies (Sivaselvan and Reinhorn, 2000; Domaneschi, 2012).

An excellent overview on the isolation knowledge, including modeling and analysis options, can be found in the research report (Grant et al., 2005). Even though not specifically oriented to NPP buildings, the report describes the main characteristics of a seismic isolation system, listing several models for the unidirectional numerical simulation. Finally, a bidirectional model is also proposed for representing the bearings response in terms of stiffness, damping and degradation, on the basis of a decomposition of the bearing resisting force as the sum of an elastic component (from Mooney–Rivlin strain energy function) and an hysteretic force. Bidirectional test data have been also employed for the calibration of the proposed model.

Kikuchi and Aiken proposed a non-differential unidirectional model for elastomeric isolation bearings (Kikuchi and Aiken, 1997), developed from the approach by Fujita. The latter is characterized by a procedure to update model parameters, this being a feature not included in classical differential models, such as the ones in (Ozdemir, 1976; Wen, 1976). The model proposed by Kikuchi and Aiken modifies the Fujita one in order to improve the performance of the model at high shear strain levels; however it neglects the effects of the strain rate and of the variation of axial load.

Hwang et al. (2002) developed an analytical unidirectional model starting from the proposal by Pan and Yang (1996). In the latter, the shear force experienced by the isolator is attributed to the sum of a restoring force, describing the skeleton curve, and a damping force, adopted to represent the area of the hysteresis loop. The model, however, is unable to describe the Mullins and the scragging effect on the bearings. The Hwang et al. proposed model for high damping elastomeric isolation devices is aimed to overcome such limits. The two components of the original Pan and Yang model have been modified to describe the degradation of stiffness and damping through a special integral term which considers the energy dissipated by the elastomeric material or bearing during cyclic loading reversals. Nevertheless the proposed approach neglects the influence of the axial load, of the rubber compound and of the vulcanization process, which can also control the hysteresis behavior of elastomeric isolation bearings. The model parameters identification is also not included in this study, which is mainly focused on the prediction of the force–displacement hysteresis.

The differential unidirectional model for HDRBs by Tsai et al. (2003) has been developed by modifying the Wen model to include rate-dependent effects under constant axial loads. However, the good correlation between experimental and numerical results does not show the stiffness and damping degradation, which is distinctive of such devices.

A nonlinear rate dependent unidirectional model for HDRBs under constant axial load is proposed by Jankowski (2003). This is a non-differential model, developed as well from the Pan and Yang (1996) solution. The cyclic experimental tests are well reproduced by the model, even though its performance gets worse when a seismic signal is applied.

Abe et al. (2004a,b) proposed differential hysteretic models of laminated rubber bearings, HDRB, lead–rubber bearings (LRB) and natural rubber bearings (NRB), under biaxial and triaxial loading conditions on the basis of experimental results. An unidirectional model is first derived by extending the Ozdemir (1976) elasto-plastic model; subsequently, a bidirectional model of the bearing is developed by including symmetric components of the characteristic matrix. This approach results accurate in the simulation of the device response also under seismic-type loading histories.

The study proposed by Ryan et al. (2005) approaches the problem of the influence of the axial load variation in the isolator horizontal stiffness and yielding strength. The following considerations has been underlined for both HDRB and LRB: (i) the lateral stiffness decreases with the increasing axial load; (ii) the lateral yield strength decreases with decreasing axial load (LRB only); (iii) the vertical stiffness decreases with increasing lateral deformation. Some considerations on the numerical modeling of HDRB and LRB devices are also included. Note that the proposed solutions,

although an improvement in the isolation knowledge, are reported by the authors as an incomplete representation of the experimental response.

The study by Yamamoto et al. (2009) proposes a two-dimensional model for the numerical simulation of seismic isolation bearings including the influence of axial load. Such model is based on an analytical approach comprising shear and axial springs, having properties which vary with the vertical load. In particular, the axial effect is captured by the material nonlinearity formulation of the axial springs and by the transversal geometric nonlinearity of the shear stiffness. A three dimensional development of this model has been reported in (Kikuchi et al., 2010); however, no evaluation of the model performance is given under three dimensional loading paths (e.g. circular or 8-shaped in the horizontal plane) and/or seismic loads.

Table 1 reports the main characteristics of the evaluated models. Among these, the approach proposed by Abe et al. (2004a,b) has been herein selected due to its good representation of the experimental response for both cyclic and seismic loading, particularly when bidirectional loading paths in the horizontal plane are considered.

4. Application to a base-isolated reactor building

IRIS is a medium power (335 MWe) pressurized light water reactor whose preliminary design has been developed by an international consortium which includes more than 20 partners from 10 countries (Carelli et al., 2004). Installation in a site characterized by a low-to-average seismicity level has been herein assumed. In a tentative design of the NSSS building (see Fig. 2a), the introduction of an isolation system was considered; the system is made by 120 HDRB devices installed between the foundation slab and the base (Fig. 2b). The isolators are made of alternated rubber layers and steel plates, bonded through vulcanization. Damping factor intrinsic to this technology ranges generally from 10% to 20%, while shear modulus lies in the 0.8–1.4 MPa range.

Steel plates give a high vertical stiffness to the isolator, though allowing large horizontal deformations. Therefore, the isolated building has low natural frequencies for motions lying in the horizontal plane, typically in the range 0.5–0.7 Hz, where the spectrum of ground motion has generally quite low energy. In such vibration modes the isolated building moves like a rigid body (see also Forni et al., 2010) over the isolators, which are strained in shear, continuously carrying the dead load. The absolute acceleration of the building can be much smaller than the *PGA*, with no amplification at higher floors. This is obtained at the price of large relative displacements between the building and the adjacent ground, this being a perspective problem for the design of the expansion joints and the connections with non isolated buildings of all the pipelines and service networks. The design of the isolation system, therefore, must reach a reasonable compromise between limitation of absolute accelerations and relative displacements. For the case of the IRIS NSSS this led to a 0.7 Hz isolation frequency, i.e. to a value which can be seen as an upper limit for the parameter: note that, for the non-isolated case the lowest natural frequency of the building, associated to a global rocking mode, is in the range 2–6 Hz according to the soil stiffness (shear modulus approximately ranging from 0.1 to 1 GPa).

In view of the above considerations, the choice of 0.7 Hz as isolation frequency, though leading to a somehow limited degree of decoupling between the structural and ground motion, is effective in limiting the relative displacement between the isolated building and the ground to a value of 10 cm at the SSE level (PGA equal to 0.3 g). This is advantageous both for the performance of the isolators in beyond design conditions and for the design of steam lines

Table 1
Main characteristics of the referenced models.

	Grant et al. (2005)	Kikuchi and Aiken (1997)	Hwang et al. (2002)	Tsai et al. (2003)	Jankowski (2003)	Abe et al. (2004b)	Ryan et al. (2005)	Yamamoto et al. (2009)	Kikuchi et al. (2010)
Dimension	Bidirectional	Unidirectional	Unidirectional	Unidirectional	Unidirectional	Uni & bidirectional	Unidirectional	Unidirectional	Bidirectional
Formulation	Differential	Non differential	Non differential	Differential	Non differential	Differential	Non differential	Non differential	Non differential
Device	HDRB	LRB–HDRB	HDRB	HDRB	HDRB	NRB–LRB–HDRB	LRB–HDRB	LRB–HDRB	LRB–HDRB
Axial load	Constant	Constant	Constant	Constant	Constant	Constant	Variable	Variable	Variable
Modified version of	–	Fujita	Pan and Yang	Wen	Pan and Yang	Ozdemir	Kelly	Kikuchi and Aiken	Yamamoto et al.
Degradation	Y	Y	Y	Y	Y	Y	N	Y	Y
Hysteretic damping	Y	Y	N	Y	N	Y	Y	Y	Y
Viscoelastic damping	Y	N	Y	Y	Y	N	N	N	N
Rate-dependent effects	Y	N	Y	Y	Y	N	N	N	N
Temperature	N	N	Y	N	N	N	N	N	N
Parameters identification	Y	Y	N	Y	Y	Y	Y	Y	Y
Cyclic loading	Y	Y	Y	Y	Y	Y	N	Y	Y
Seismic loading	N	Y	Y	N	N	Y	N	Y	N

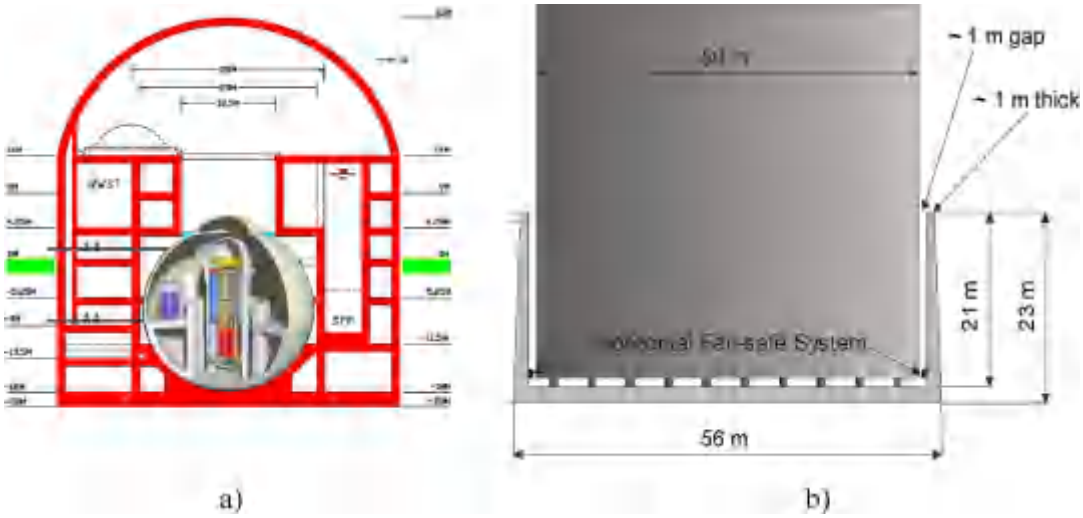

Fig. 2. (a) IRIS reactor building main section; (b) schematic view of the IRIS isolation system.

connecting the NSSS building with the turbine units. If some equipment component (e.g. some wide span pipeline) has a lower natural frequency a local specific measure (stiffening or energy dissipation device) must be adopted.

The characteristics of the isolators are given in Table 2 (½ scaled for laboratory tests and real dimensions). The resulting natural frequencies of the NPP isolated model are given in the Appendix (for comparison with the IRIS non isolated version see also De Grandis et al., 2009).

4.1. Mechanical modeling assumptions and criteria

To compute the dynamic response of the IRIS reactor building a 6-DOF 3D-model has been implemented in Matlab (2008) under the hypothesis that the isolated superstructure behaves like a rigid body; soil–structure interaction has been neglected.

In the Appendix the dynamic equilibrium equations of the 6-DOF model are given; these are consistent to the hypothesis that the behavior of isolators under horizontal and vertical loading is independent. In fact, it was assumed that HRDB devices are linear elastic under vertical loading, showing the same stiffness in tension and compression; their non linear behavior under horizontal loading has been modeled accordingly to the bidirectional approach by Abe et al. (2004b). Therefore, the restoring force for the HDRB device is the sum of three contributions, i.e. an elastic–plastic model (F_2 hysteretic component) and two elastic non-linear springs, namely a non-linear elastic spring (F_1) and an hardening spring (F_3). In light of these observations the resulting scheme is represented in Fig. 3a.

Table 2
Characteristics of the tested isolator (in brackets real life dimensions).

Isolator external diameter, d	500 (1000) mm
Steel reinforcing plate diameter, d'	480 (980) mm
Thickness of internal steel plates, t_s	2 (4) mm
Number of elastomeric layers, n	10
Thickness of elastomeric layers, t_r	5 (10) mm
Total elastomeric thickness, T_r	50 (100) mm
First shape factor, $S_1 = d'/4t_r$	24.0 (24.5)
Second shape factor, $S_2 = d'/nt_r$	9.60 (9.80)
Full isolator height, T_b	128 (195) mm
Nominal dynamic shear modulus, G	1.4 MPa
Hardness	75 Shore A3
Nominal damping factor	10%/15%

From an analytical point of view the force–displacement relation for the first non-linear spring reads:

$$F_1 = K_1 \left[\beta + (1-\beta)\exp\left(-\frac{U_{\max}}{\alpha}\right)\right] U + a[1-\exp(-b|U|)]sgn(U) \tag{9}$$

where U is the relative displacement while K_1, a and b are parameters. In Eq. (9), the first term reproduces the force linear evolution, while the second one the non-linear behavior.

The hysteretic contribution F_2 is described by the following differential equation:

$$\dot{F}_2 = \frac{Y_t}{U_t}\left[\dot{U} - |\dot{U}|\left|\frac{F_2}{Y_t}\right|^n sgn\left(\dot{U}\frac{F_2}{Y_t}\right)\right] \tag{10}$$

where the Y_t and U_t parameters are in turn defined as:

$$Y_t = Y_0\left[1 + \left|\frac{U}{U_H}\right|^p\right] \qquad U_t = U_0\left[1 + \frac{U_{\max}}{U_S}\right] \tag{11}$$

being Y_0 is the initial yielding force, U_0 the initial yielding displacement, U_H the displacement where hardening starts, U_S a parameter for controlling the degradation of the elastic stiffness of the elasto-plastic spring, U_{max} the maximum displacement experienced during the loading history and p a parameter governing the shape of the hardening branch.

Finally a further non-linear spring is introduced in parallel for capturing the increment of the tangential stiffness experienced by the devices at very high strain levels. This results in the F_3 contribution (Fig. 3b), defined as:

$$F_3 = K_2\left|\frac{U}{U_H}\right|^r U \tag{12}$$

where r is the parameter to prescribe the shape of the hardening curve, K_2 a constant to describe the contribution of the hardening spring to the total stiffness.

In Fig. 3b the contributions of the three component forces is highlighted for a cyclic experimental test on a reference specimen as force–displacement diagram up to displacement values of the 300% rubber height.

Experimental tests of the behavior of the adopted HDRB devices under imposed cyclic relative displacements and constant axial force have been carried on within the IRIS project activity. Due to the very large dimensions of the HDRB elastomeric devices specifically designed for the IRIS reactor building, standard tests on ½ scaled HDRB seismic isolator prototypes (see Table 2) have been

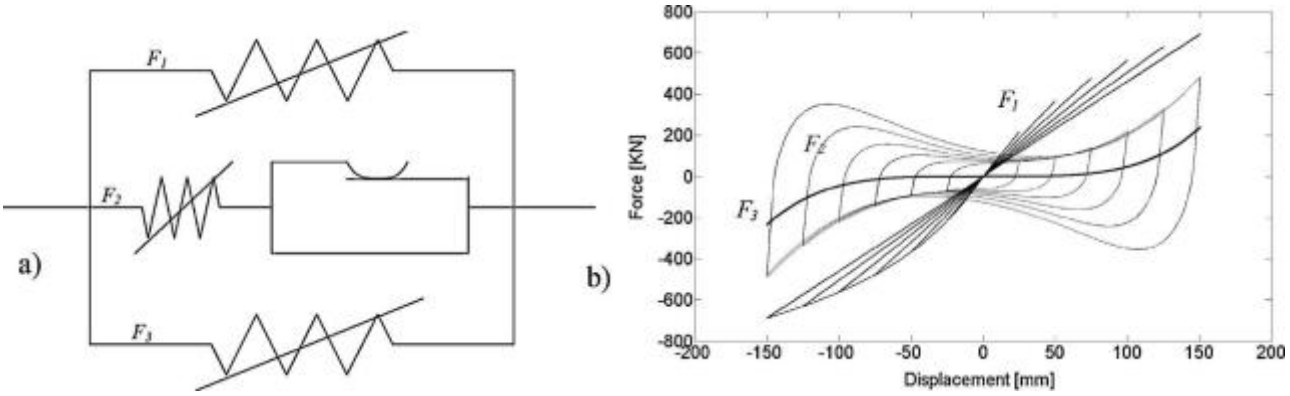

Fig. 3. (a) Scheme of the Abe et al. model; (b) force components under cyclic loading.

performed in two phases by the CESI-ISMES LPS (www.cesi.it) laboratory in Seriate (Italy) and by the FIP (www.fip-group.it) laboratory in Selvazzano Dentro (Italy).

Six isolators were tested in two sessions. The first comprised vertical loading tests, horizontal loading tests in static and dynamic conditions (ramped and sinusoidal control input). In this step the average shear deformation exceeded by 1.5 times the design one (100%) (see report ENEA, 2010a for details). The second session aimed at investigating isolator failure and comprised a vertical loading failure test and a horizontal cyclic quasi-static loading failure test (ENEA, 2010b). A vertical failure mode consisting in the expulsion of the rubber internal plates, along the radial direction, from the external steel plates at 45,500 KN load level (corresponding to 215 MPa average compression stress) has been shown. Horizontal failure at constant vertical load (2000 kN) has been investigated by imposing cyclic shear displacements to a couple of devices (installed in a double-shear configuration and parallel connection) corresponding to shear strain values of ±50%, ±100%, ±150%, ±200%, ±250%, ±300%, with 1 mm/s test rate. The last cycle at a rubber shear strain of 350% has been finally imposed in one way for safety issues, being the actuator capacity reached (80 MN test rig). In such conditions, isolators did not show any sign of failure. Aiming to reach failure, applying higher values of horizontal displacements, a single isolator configuration has been also evaluated on the same test facility and axial load. First damage occurred at a shear strain level close to 400%.

Fig. 4 (thin line) depicts a typical representative outcome of a cyclic shear tests at FIP laboratory in quasi-static conditions; this test results have been adopted as the experimental target for calibrating the numerical model parameters (Abe et al., 2004b).

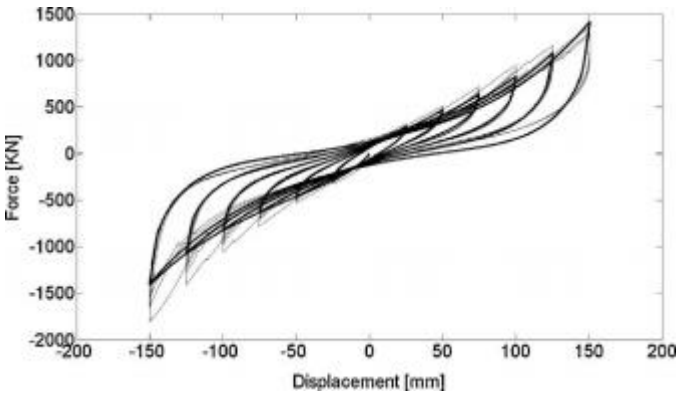

Fig. 4. Cyclic shear test of the tested isolator in quasi-static condition (50%, 100%, 150%, 200%, 250%, 300% deformations and 2000 kN constant axial force). Thin line, experimental test; thick line, numerical simulation.

The resulting values (corresponding to the thick line in Fig. 4) are the following: $K_1 = 10{,}000$ kN/m; $\alpha = 0.1$ m; $\beta = 0.3$; $a = 4.87$ kN; $b = 60\ \mathrm{m}^{-1}$; $n = 0.36$; $Y_0 = 70$ kN; $U_h = 0.06$ m; $p = 2.4$; $U_0 = 0.006$ m; $U_s = 0.05$ m; $K_2 = 100$ kN/m; $r = 3$. For an appreciation of the model capabilities in terms of representation of the hysteretic response, in Fig. 5 numerical results (thick line) are compared to the experimental behavior (thin line) for cycles at 100% and 250% shear deformation (respectively Fig. 5a and b).

Table 3 reports the quantitative comparison between the experimental results and the numerical fitting performed in terms of secant stiffness and damping factor; the first is computed at the cycle peak displacement, the second from the area of the hysteretic curve. The overall picture of the results appears satisfactory even though damping looks slightly overestimated with respect to experimental data.

4.2. Random variables and experimental design

Moving on the implementation of the IRIS NPP isolation system, and, consequently, considering the real life dimensions for the HDRB devices, a very limited number of random variables has been considered to illustrate the proposed procedure, controlling the stiffness and dissipation properties of the devices and their displacement at collapse. More precisely, three random variables have been selected and characterized according to the following criteria.

- X_1, used to control the stiffness of the isolator model, multiplies the values of the stiffness parameters K_1, a (Eq. (9)), and K_2 (Eq. (12)) and divides the value of the initial yielding displacement U_0 in Eq. (10). This random variable has lognormal distribution with unit mean (leading to the values obtained by fitting the experimental response) and c.o.v. equal to 0.22.
- X_2, used to control the damping of the isolator, multiplies the value the initial yielding force Y_0. This random variable has the same distribution as x_1.
- $X_1 \equiv U_f$, the relative displacement leading to failure of the most strained isolator, has been assumed as lognormal, with a mean value equal to four times the rubber thickness (400% average shear deformation) and variable c.o.v. (0.05, 0.1, 0.2).

Note that, since independent control of stiffness and damping is impossible in the adopted model, a numerical sensitivity analysis has been performed on the unidirectional model (Abe et al., 2004b). Extensive cyclic simulations have been carried on, adopting different values for X_1 and X_2, for evaluating the secant stiffness and equivalent damping variation. In Table 4 some results are summarized, showing how for increasing value of the X_1 variable the overall stiffness increases, while damping decreases; increasing X_2,

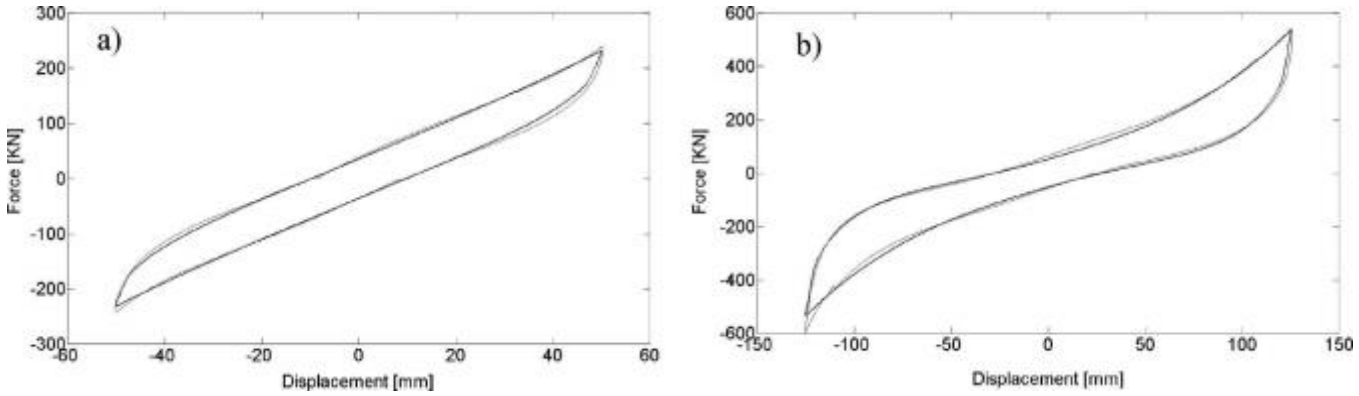

Fig. 5. Tested isolator phenomenological model: comparison of experimental (thin line) and numerical (thick line) behavior. (a) second cycle, (b) fifth cycle.

Table 3
Quantitative comparison between the laboratory experimental results (tested isolator) and the Abe et al. (2004b) model fitting.

	Shear deformation (%)	Experimental		Numerical	
		Equivalent viscous damping factor (%)	Secant stiffness (kN/mm)	Equivalent viscous damping factor (%)	Secant Stiffness (kN/mm)
1° Cycle	50	11.05	5.83	11.63	5.68
2° Cycle	100	9.54	4.72	9.07	4.60
3° Cycle	150	8.78	4.47	8.58	4.17
4° Cycle	200	8.69	4.46	8.82	4.10
5° Cycle	250	8.80	4.53	9.22	4.26
6° Cycle	300	8.38	4.68	9.61	4.64

Table 4
Sensitivity analysis on the Abe et al. (2004b) unidirectional model (real life dimensions).

	$X_1 = 1$		$X_1 = 1.2$		$X_1 = 1.6$	
	Damping factor (%)	Secant stiffness (kN/mm)	Damping factor (%)	Secant stiffness (kN/mm)	Damping factor (%)	Secant stiffness (kN/mm)
1° Cycle	11.56	11.4	10.6	13.1	9	16.5
2° Cycle	9.07	9.21	8.1	10.7	6.6	13.6
3° Cycle	8.69	8.35	7.7	9.7	6.3	12.4
4° Cycle	8.82	8.2	7.8	9.5	6.4	12
5° Cycle	9.26	8.53	8.2	9.8	6.7	12.3
6° Cycle	9.61	9.28	8.5	10.6	7	13.3
	$X_2 = 1$ Damping factor (%)	Secant stiffness (kN/mm)	$X_2 = 1.2$ Damping factor (%)	Secant stiffness (kN/mm)	$X_2 = 1.6$ Damping factor (%)	Secant stiffness (kN/mm)
1° Cycle	11.56	11.4	13.2	12	16	13.1
2° Cycle	9.07	9.21	10.4	9.5	13	10.3
3° Cycle	8.69	8.35	10	8.7	12.2	9.4
4° Cycle	8.82	8.2	10	8.6	12.2	9.5
5° Cycle	9.26	8.53	10.4	9	12.5	10.1
6° Cycle	9.61	9.28	10.4	9.9	12.7	11.2

on the other hand, makes damping increase significantly, with a more limited growth of the secant stiffness.

Table 5 lists the values adopted for X_1 and X_2 according to the experimental design for estimating the coefficients of the Response Surfaces (which are independent of X_3). This values have been selected according to a Central Composite Design (CCD) strategy and to the following criteria.

- The initial design center is assumed at the mean values of the random variables.
- The high-low levels of the CCD correspond to 1% and 99% exceedance probability in the lognormal statistics.
- Given that $\eta_i = (x_i - \mu_{xi})/\sigma_{xi}$, and for fulfilling the rotatability property (Draper and Smith, 1981) the "star points" are located at $\eta_i = \pm\sqrt[4]{2^k}$, being k the number of random variables.

Table 5
Design of experiments.

Exp.	X_1	X_1
1	1	1
2	1	0.689
3	1	1.311
4	0.689	1
5	1.311	1
6	1.61	0.59
7	0.59	1.61
8	0.59	0.59
9	1.61	1.61

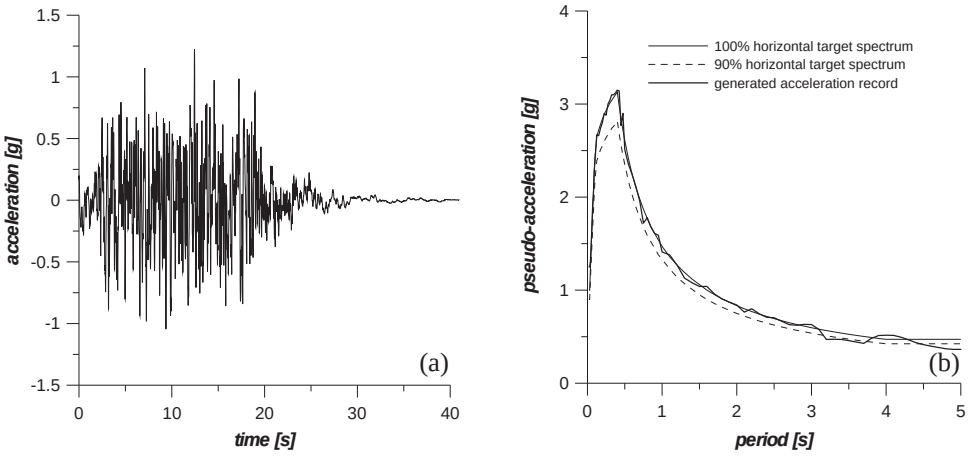

Fig. 6. Example of artificial accelerogram (a) and comparison with the USNRC spectrum (b).

4.3. Computation of fragility and risk

Fragility analysis was performed by assuming, as seismic excitation, twenty sets of artificial accelerograms, each set encompassing three independent components of ground motion. Accelerograms were generated in order to be compatible to the USNRC 1.60 response spectra (USNRC, 1973). In Fig. 6 an example of artificial accelerogram is given together with the comparison of its pseudo-acceleration spectrum to the target curve.

Accordingly to the procedure described at Section 2, given a fixed ground shaking intensity level (*PGA*), the following steps have been performed.

1. At each experimental point (see Table 5):
   (a) dynamic step-by-step analysis has been run for all realizations of the ground excitation and the extreme value u of the relative displacement (in horizontal plane) among all devices has been computed;
   (b) the mean value and standard deviation of the extreme value u among all realizations have been computed (see Table 6).
2. The coefficients of the Response Surfaces (7) have been estimated via Least Square analysis; from these the variation with X of the mean and standard deviation of u is known. With standard manipulation, the corresponding variation of the parameters α, β has been derived, defining the following conditioned I type extreme-value distribution

$$P_{U|1,\ldots,m}(u|x_1, \ldots, x_m) = \exp[-\exp(-\alpha(x_1, \ldots, x_m) \times (u - \beta(x_1, \ldots, x_m)))] \quad (13)$$

3. Once the conditioned distribution function (13) is stated and the density function for all random variables are specified, the integral (6) can be evaluated via direct Monte Carlo analysis.

The results of the performed fragility analysis are given in Fig. 7 for different values of the coefficient of variation of the relative displacement at failure (U_f). It can be observed how the spreading of the displacement at failure (maximum c.o.v. of 0.2) increases significantly the probability of exceeding the limit state for *PGA* values up to three times the design level. Conversely, when higher excitation levels have been considered, some benefits with regard to fragility can be found. Subsequent computations, devoted to the estimation of the overall risk associated to the isolators collapse, were performed by assuming a c.o.v. of 0.1 for the displacement at failure.

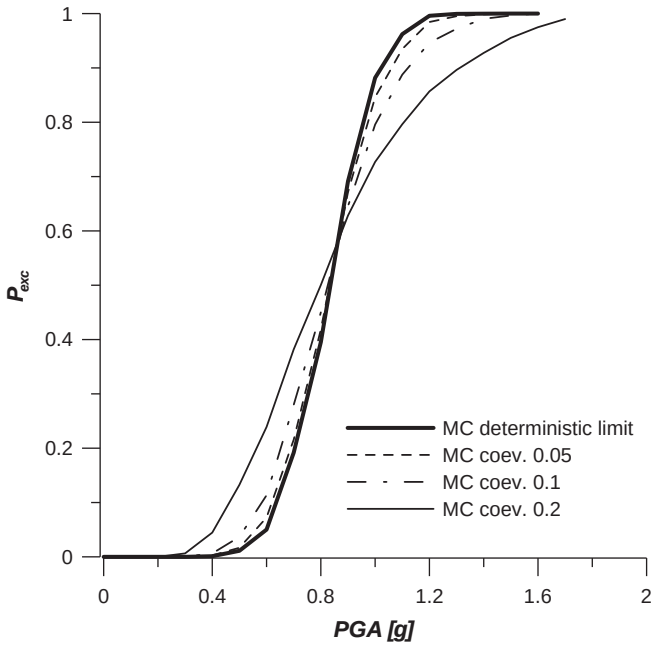

Fig. 7. Fragility curves for different values of the c.o.v. of U_f.

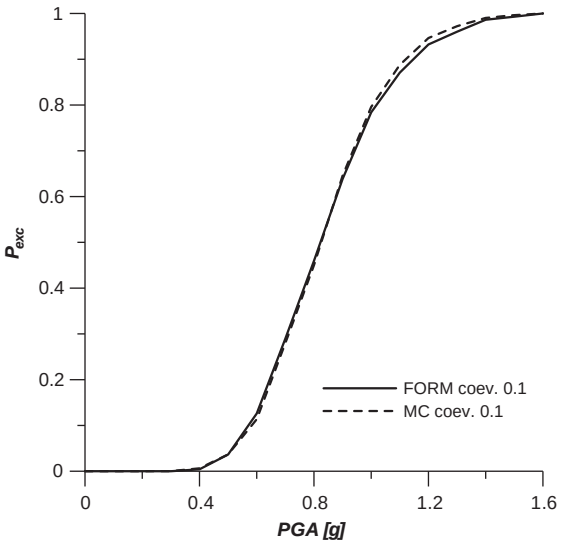

Fig. 8. Comparison between Monte Carlo and FORM results.

Table 6
Mean value and standard deviation of the relative displacement across the most strained isolator among all realizations.

Exp.	0.3 g		0.4 g		0.5 g		0.6		0.7 g		0.8 g	
	μ_U	σ_U	μ_U	σ_U	μ_U	σ_U	μ_U	σ_U	μ_U	σ_U	μ_U	σ_U
1	0.219	0.016	0.263	0.021	0.301	0.026	0.333	0.025	0.364	0.026	0.395	0.031
2	0.240	0.020	0.287	0.022	0.332	0.025	0.361	0.029	0.394	0.031	0.426	0.029
3	0.201	0.016	0.246	0.021	0.281	0.026	0.311	0.027	0.339	0.030	0.361	0.030
4	0.243	0.025	0.289	0.028	0.328	0.030	0.357	0.032	0.389	0.032	0.413	0.034
5	0.207	0.018	0.247	0.020	0.281	0.019	0.313	0.018	0.349	0.022	0.372	0.016
6	0.228	0.021	0.287	0.028	0.327	0.025	0.361	0.023	0.408	0.035	0.444	0.046
7	0.222	0.021	0.264	0.023	0.301	0.022	0.336	0.021	0.366	0.027	0.391	0.034
8	0.281	0.022	0.332	0.030	0.371	0.033	0.418	0.038	0.452	0.036	0.472	0.043
9	0.163	0.015	0.209	0.017	0.245	0.018	0.273	0.019	0.300	0.019	0.324	0.021

Exp.	0.9 g		1.0 g		1.1 g		1.2 g		1.3 g		1.4 g		1.5 g	
	μ_U	σ_U	μ_U	σ_U	μ_U	σ_U	μ_U	σ_U	μ_U	σ_U	μ_U	σ_U	μ_U	σ_U
1	0.412	0.027	0.436	0.033	0.466	0.039	0.490	0.043	0.514	0.042	0.526	0.042	0.560	0.037
2	0.460	0.029	0.489	0.039	0.518	0.039	0.544	0.042	0.580	0.052	0.605	0.044	0.626	0.052
3	0.389	0.032	0.413	0.029	0.436	0.029	0.460	0.033	0.481	0.033	0.507	0.032	0.527	0.036
4	0.439	0.028	0.472	0.033	0.492	0.042	0.516	0.043	0.534	0.048	0.557	0.048	0.586	0.047
5	0.402	0.026	0.428	0.032	0.451	0.037	0.479	0.035	0.498	0.043	0.516	0.034	0.538	0.031
6	0.490	0.044	0.515	0.048	0.536	0.041	0.544	0.039	0.564	0.032	0.570	0.036	0.614	0.046
7	0.416	0.033	0.442	0.034	0.464	0.034	0.483	0.038	0.503	0.037	0.518	0.043	0.539	0.043
8	0.514	0.042	0.544	0.056	0.573	0.040	0.609	0.041	0.652	0.054	0.655	0.064	0.723	0.061
9	0.350	0.022	0.373	0.025	0.392	0.026	0.416	0.027	0.435	0.026	0.457	0.029	0.471	0.034

Under this assumption, in Fig. 8 the results obtained via Monte Carlo simulation are first compared to the ones computed by the FORM approach and the Rosenblatt Transformation, showing a remarkable level of agreement between the two procedures.

As pointed out in Section 2.3, given an initial estimate of the fragility curve, an "informative" risk analysis can be performed for a prototype site. To this aim a site has been considered, which is characterized, in terms of seismic hazard, by the *PGA*-return period curve of Fig. 9, where a 0.3 g level corresponds to a return period of 10^4 years. From this, the probability density function of the annual *PGA* has been derived and the integrand function in Eq. (8) has been computed. This is given in Fig. 10, clearly showing the range of the ground shaking level mostly contributing to the total seismic risk.

In commenting these results, which are also affected by the limited number of random variables considered, it must be observed that the failure criterion based on relative displacement across the isolators does not account for the effect of the axial force variation, which can be very important for buildings of this type. In this light the adoption of a limit state surface as the one sketched in Section 2.2 seems to be advisable, even though it requires extensive experimental investigation.

Nevertheless, it seems possible to draw a few general comments on of the results in Fig. 10.

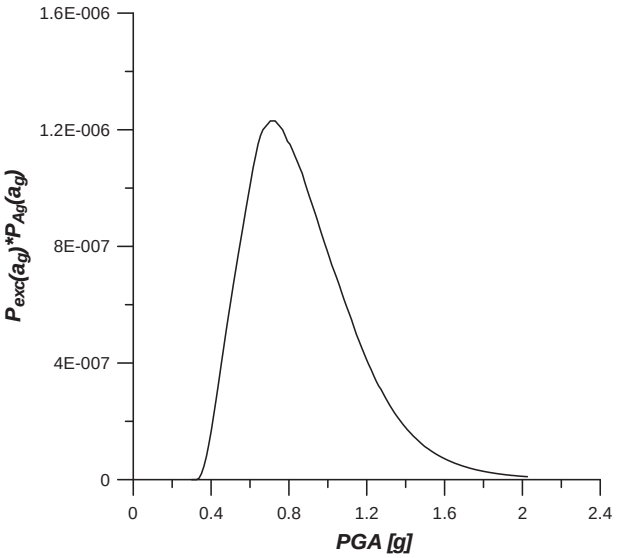

Fig. 10. Integrand function delivering annual probability of failure.

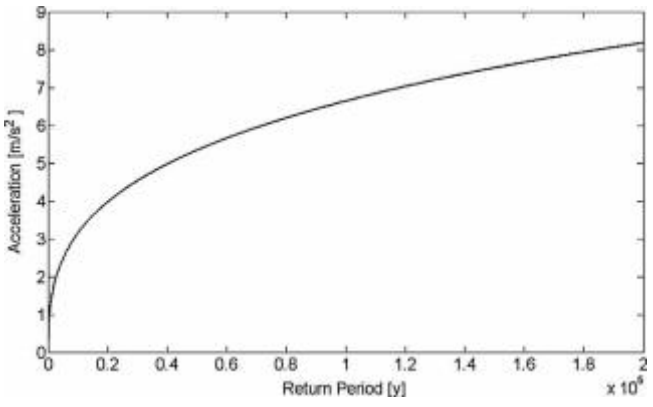

Fig. 9. Seismic hazard: *PGA* versus return period.

- The definition of a significant "beyond design" PGA level equal to three times the design value seems to be supported by the integrand risk curve here computed, having a "centroid" not far from 0.9 g, 0.3 g being the design PGA.
- This results is rather similar to the one obtained in (De Grandis et al., 2009), in completely different structural conditions but for the same site, by working on a non-isolated version of the IRIS reactor building. Risk was associated, in that case, to the reaching of an "excessive" acceleration value at a point where a safety component inside the vessel was fixed.

5. Conclusions

A numerical procedure has been proposed for evaluating the fragility of base-isolated NPP buildings under the hypothesis that isolation devices are the critical elements when the overall seismic risk is considered.

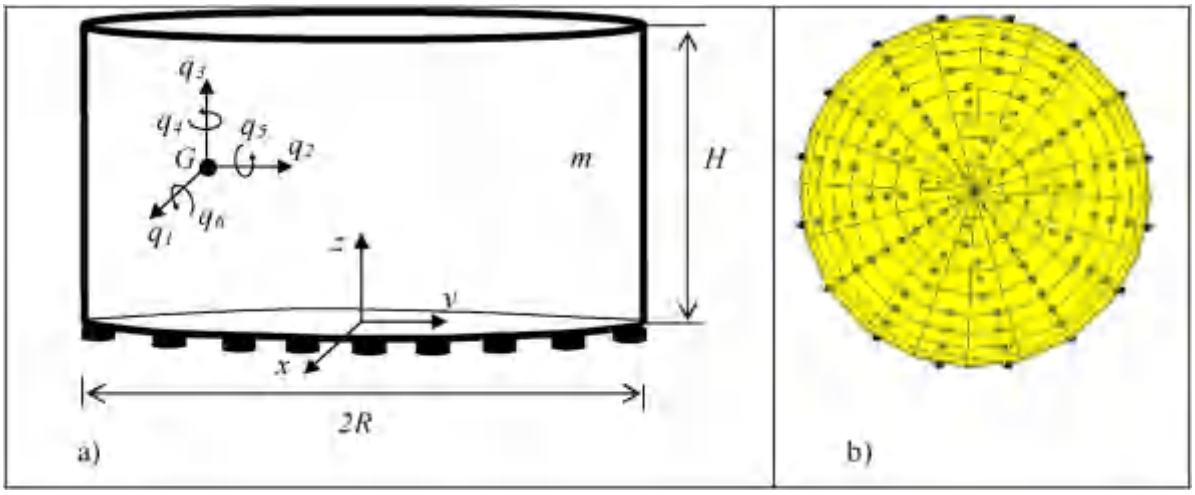

Fig. A1. Isolated NPP dynamical model: (a) coordinate system, (b) layout of isolators.

The procedure, based on step-by-step dynamic integration, Response Surface Methodology, 1st order reliability methods and Monte Carlo Simulation, implements a refined approach for modeling the non-linearity of the mechanical behavior of isolators, this being a fundamental aspects when beyond-design conditions are addressed. On the other hand, the inherent simplification of the structural behavior of the building, herein implemented with a rigid-body motion approach, stemming from the introduction of the isolation system, is exploited to reduce the computational effort.

An example of application is shown regarding the application of HDRB isolators to the NSSS building within the IRIS international project; a small number of random variables has been considered for characterizing the isolators cyclic behavior and their ultimate deformability. As a natural extension, random variables describing the structural properties (e.g. effective stiffness of r.c. members) and the excitation process can be easily accounted for.

Acknowledgements

The authors gratefully thank Professor Leone Corradi dell'Acqua of the Department of Energy of Politecnico di Milano for his precious help and encouragement. Giorgio Bianchi and Davide Mantegazza are also gratefully acknowledged for their effective support. This work has been partially sponsored by CIRTEN under the ENEA-MSE (Ministry for Economic Development) protocol of June 21, 2007.

Appendix A.

With reference to Fig. A1, the equations of motion of the 3D IRIS base isolated NPP model with 6 degrees of freedom are presented by following the Lagrangian approach. Coordinates q_1, q_2, q_3 represent displacement components, parallel to the global reference system x, y, z. Coordinates q_4, q_5, q_6 are rotations around respectively, q_3, q_2, q_1 directions.

Table A1.

Table A1
Natural frequencies of the vibration modes of the model.

Mode	Natural frequency (Hz)	Mode description
1	0.68	Rotation about q_3 vertical axis
2	0.69	q_1 Horizontal translation
3	0.69	q_2 Horizontal translation
4	12.7	Rocking about q_2 horizontal axis
5	12.7	Rocking about q_1 horizontal axis
6	17.1	q_3 Vertical translation

The following equations of motion arise:

$$m\ddot{q}_1 + \sum_{i=1}^{n} F_{f1i} = -ma_{h1} \tag{A1}$$

$$m\ddot{q}_2 + \sum_{i=1}^{n} F_{f2i} = -ma_{h2} \tag{A2}$$

$$m\ddot{q}_3 + k_v n q_3 - k_v \sum_{i=1}^{n} (x_i - x_G) q_5 + k_v \sum_{i=1}^{n} (y_i - y_G) q_6 + c_v n \dot{q}_3 - c_v \sum_{i=1}^{n} (x_i - x_G) \dot{q}_5 + c_v \sum_{i=1}^{n} (y_i - y_G) \dot{q}_6 = -ma_v \tag{A3}$$

$$I_{G1}\ddot{q}_4 - \sum_{i=1}^{n} F_{f1_i}(y_i - y_G) + \sum_{i=1}^{n} F_{f2_i}(x_i - x_G) = 0 \tag{A4}$$

$$I_{G2}\ddot{q}_5 - z_G \left[\sum_{i=1}^{n} F_{f1_i} - k_v \sum_{i=1}^{n} (x_i - x_G) q_3 + k_v \sum_{i=1}^{n} (x_i - x_G)^2 q_5 - k_v \sum_{i=1}^{n} (x_i - x_G)(y_i - y_G) q_6 - c_v \sum_{i=1}^{n} (x_i - x_G) \dot{q}_3 + c_v \sum_{i=1}^{n} (x_i - x_G)^2 \dot{q}_5 - c_v \sum_{i=1}^{n} (x_i - x_G)(y_i - y_G) \dot{q}_6 = 0 \right] \tag{A5}$$

$$I_{G3}\ddot{q}_6 + z_G \left[\sum_{i=1}^{n} F_{f2_i} + k_v \sum_{i=1}^{n} (y_i - y_G) q_3 - k_v \sum_{i=1}^{n} (x_i - x_G)(y_i - y_G) q_5 + k_v \sum_{i=1}^{n} (y_i - y_G)^2 q_6 + c_v \sum_{i=1}^{n} (y_i - y_G) \dot{q}_3 - c_v \sum_{i=1}^{n} (x_i - x_G)(y_i - y_G) \dot{q}_5 + c_v \sum_{i=1}^{n} (y_i - y_G)^2 \dot{q}_6 = 0 \right] \tag{A6}$$

where coordinates with "*G*" subscript are relative to the system centroid, and where the following symbols apply.

F_{f1_i} and F_{f2_i}	are the horizontal restoring forces exerted by the *i*th isolator,
k_v, c_v	are the isolator vertical stiffness and damping coefficients,
m, I_{G_1}, I_{G_2}, I_{G_3}	are the mass and moments of inertia of the isolated portion of the building,
a_{h1}, a_{h2}, a_v	are the components of ground acceleration.

References

Abe, M., Yoshida, J., Fujino, Y., 2004a. Multiaxial behaviors of laminated rubber bearings and their modeling: I. Experimental study. J. Struct. Eng. ASCE 130, 1119–1132.

Abe, M., Yoshida, J., Fujino, Y., 2004b. Multiaxial behaviors of laminated rubber bearings and their modeling: II. Modeling. J. Struct. Eng. ASCE 130, 1133–1144.

American Society of Civil Engineers (ASCE), 2000. Seismic Analysis of Safety-Related Nuclear Structures and Commentary. ASCE 4-98. ASCE, Reston, VA.

American Society of Civil Engineers (ASCE), 2005. Seismic Design Criteria for Structures, Systems, and Components in Nuclear Facilities. ASCE/SEI 43-05. ASCE, Reston, VA.

Bianchi, G., Corradi, L., Domaneschi, M., Mantegazza, D.C., Perotti, F., Ravez, A., 2011a. Limit state domain of high damping rubber bearings in seismic isolated nuclear power plants. In: 21st International Conference on Structural Mechanics in Reactor Technology (SMIRT-21), New Delhi, India, Paper ID 205.

Bianchi, G., Corradi Dell'Acqua, L., Domaneschi, M., Mantegazza, D., Perotti, F., 2011b. A procedure for the computation of seismic fragility of NPP buildings with base isolation. In: International Topical Meeting on Probabilistic Safety Assessment and Analysis (PSA2011), Wilmington, NC, USA, ISBN 978-0-89448-089-8.

Bianchi, G., Corradi Dell'Acqua, L., Domaneschi, M., Mantegazza, D., Perotti, F., 2011c. Limit state domain of high damping rubber bearings in seismic isolated nuclear power plants. In: 21st International Conference on Structural Mechanics in Reactor Technology (SMIRT-21), New Delhi, India, Paper ID 205.

Bucher, C.G., Burgund, U., 1990. A fast and efficient response surface approach for structural reliability problems. Struct. Saf. 7, 57–66.

Carelli, M.D., Conway, L.E., Oriani, L., Petrović, B., Lombardi, C.V., Ricotti, M.E., Barroso, A.C.O., Collado, J.M., Cinotti, L., Todreas, N.E., Grgić, D., Moraes, M.M., Boroughs, R.D., Ninokata, H., Ingersoll, D.T., Oriolo, F., 2004. The design and safety features of the IRIS reactor. Nucl. Eng. Des. 230, 151–167.

Casciati, F., Faravelli, L., 1991. Fragility Analysis of Complex Structural Systems. Research Studies Press Ltd., Taunton, Somerset, England.

Cornell, C.A., Krawinkler, H., 2000, Spring. Progress and Challenges in Seismic Performance Assessment. PEER Center News http://peer.berkeley.edu/news/2000spring/index.html

Corradi, L., Domaneschi, M., Guiducci, C., 2009. Assessing the reliability of seismic base isolators for innovative power plant proposals. In: 20th International Conference on Structural Mechanics in Reactor Technology (SMIRT20), Espoo Finland, ISBN: 978-951-38-6337-1, 978-951-38-6338-8.

De Grandis, S., Domaneschi, M., Perotti, F., 2009. A numerical procedure for computing the fragility of NPP components under random seismic excitation. Nucl. Eng. Des. 239, 2491–2499.

Der Kiureghian, A., 2005. Non-ergodicity and PEER's framework formula. Earthquake Eng. Struct. Dyn. 34, 1643–1652.

Domaneschi, M., 2012. Simulation of controlled hysteresis by the semi-active Bouc-Wen model. Comput. Struct. 106/107, 245–257.

Draper, N., Smith, H., 1981. Applied Regression Analysis. John Wiley & Sons.

ENEA, 2010a. Centro Ricerche Bologna, Report XCESI-LP-001.

ENEA, 2010b. Centro Ricerche Bologna, Report XFIP-LP2-001.

Faravelli, L., 1989. Response surface approach for reliability analysis. ASCE J. Eng. Mech. 115, 2763–2781.

Forni, M., Poggianti, A., Bianchi, F., Forasassi, G., Lo Frano, R., Pugliese, G., Perotti, F., Corradi dell'Acqua, L., Domaneschi, M., Carelli, M.D., Ahmed, M.A., Maioli, A., 2010. Seismic Isolation of the IRIS Nuclear Plant, vol. 8. American Society of Mechanical Engineers, Pressure Vessels and Piping Division, pp. 289–296.

Grant, D.N., Fenves, G.L., Auricchio, F., 2005. Modelling and Analysis of High-Damping Rubber Bearings for the Seismic Protection of Bridges. Research Report No. ROSE-2005/01. ROSE School, Pavia, I.

Hoenbichler, M., Rackwitz, R., 1981. Nonnormal dependent vectors in structural safety. ASCE J. Eng. Mech. 114, 2195–2199.

Huang, Y.N., Whittaker, A.S., Kennedy, R.P., Mayes, R.L., 2012. Response of base-isolated nuclear structures for design and beyond design basis earthquake shaking. Earthquake Eng. Struct. Dyn. (in press).

Hwang, J.S., Wu, J.D., Pan, T.C., Yang, G., 2002. A mathematical hysteretic model for elastomeric isolation bearings. Earthquake Eng. Struct. Dyn. 31, 771–789.

Jankowski, R., 2003. Nonlinear rate dependent model of high damping rubber bearing. Bull. Earthquake Eng. 1, 397–403.

Kennedy, R.P., Cornell, C.A., Campbell, R.D., Kaplan, S., Perla, H.F., 1980. Probabilistic seismic safety study of an existing nuclear power plant. Nucl. Eng. Des. 59, 315–338.

Kennedy, R.P., Ravindra, M.K., 1984. Seismic fragilities for nuclear power plant risk studies. Nucl. Eng. Des. 79, 47–68.

Kikuchi, M., Aiken, I.D., 1997. An analytical hysteresis model for elastomeric seismic isolation bearings. Earthquake Eng. Struct. Dyn. 26, 215–231.

Kikuchi, M., Nakamura, T., Aiken, I.D., 2010. Three-dimensional analysis for square seismic isolation bearings under large shear deformations and high axial loads. Earthquake Eng. Struct. Dyn. 39, 1513–1531.

Lin, D.K.J., Tu, W., 1995. Dual response surface optimization. J. Qual. Technol. 21, 34–39.

Matlab, 2008. The Language of Technical Computing Version 7.7.0.471.

Ozdemir, H., 1976. Nonlinear Transient Dynamic Analysis of Yielding Structures. Division of Structural Engineering and Structural Mechanics, Department of Civil Engineering, University of California, Berkeley (Ph.D. Dissertation).

Pan, T.C., Yang, G., 1996. Nonlinear analysis of base-isolated MDOF structures. In: Proceedings of the 11th World Conference on Earthquake Engineering, Mexico, Paper No. 1534.

Pinto, P.E., Giannini, R., Franchin, P., 2004. Seismic Reliability Analysis of Structures. IUSS Press, Pavia, Italy.

Rajashekhar, M.R., Ellingwood, B.R., 1993. A new look at the response surface approach for reliability analysis. Struct. Saf. 12, 205–220.

Ryan, K.L., Kelly, J.M., Chopra, A., 2005. Nonlinear model for lead–rubber bearings including axial-load effects. J. Struct. Eng. ASCE 131, 1270–1278.

Sivaselvan, M.V., Reinhorn, A.M., 2000. Hysteretic models for deteriorating inelastic structures. J. Eng. Mech. ASCE 126 (6), 633–640.

Towashiraporn, P., 2004. Building seismic fragilities using response surface metamodels. Civil and Environmental Engineering, Georgia Institute of Technology (Thesis in partial fulfillment of Ph.D. degree).

Tsai, C.S., Chiang, T.C., Chen, B.J., Lin, S.B., 2003. An advanced analytical model for high damping rubber bearings. Earthquake Eng. Struct. Dyn. 32, 1373–1387.

USNRC, 1.60, 1973. Design Response Spectra for Seismic Design of Nuclear Power Plant: Regulatory Guide. US Atomic Energy Commission.

Wen, Y.K., 1976. Method for random vibration of hysteretic systems. J. Eng. Mech. ASCE 102., 249–263.

Yamamoto, S., Kikuchi, M., Ueda, M., Aiken, I.D., 2009. A mechanical model for elastomeric seismic isolation bearings including the influence of axial load. Earthquake Eng. Struct. Dyn. 38, 157–180.